



Focussed ion beam preparation and in situ nanoscopic study of Precambrian acritarchs

André Kempe^{a,1}, Richard Wirth^b, Wladyslaw Altermann^{c,*},
Robert W. Stark^a, J. William Schopf^d, Wolfgang M. Heckl^a

^a *Department für Geo- und Umweltwissenschaften, Sektion Kristallographie, Ludwig-Maximilians-Universität München, Theresienstr. 41, D-80333 München, Germany*

^b *GeoForschungsZentrum, Sektion 4.1, Telegrafenberg, D-14473 Potsdam, Germany*

^c *Centre Biophysique Moleculaire (CBM), CNRS (Centre National de la Recherche Scientifique), Rue Charles-Sadron, 45071 Orleans Cedex 2, France*

^d *Department of Earth and Space Sciences, Institute of Geophysics and Planetary Physics, University of California, Los Angeles, CA 90095-1567, USA*

Received 10 December 2004; received in revised form 4 July 2005; accepted 14 July 2005

Abstract

The taphonomic nanostructure of acritarch cell walls from the c. 650 million years old Chichkan Formation was studied with optical microscopy (OM), Raman spectroscopy, scanning electron microscopy (SEM), atomic force microscopy (AFM), and transmission electron microscopy (TEM). The integration of high-resolution methods and classical optical microscopy allows for the assessment of the relationship of the fossil to the embedding chert and of the authenticity of the fossil. Partial etching of paleontological (150 µm) and petrographic (30 µm) thin sections rather than maceration of the semi-stable cell structures served as the preparation method suitable for AFM and SEM studies. Focussed Ion Beam (FIB) preparation of sections normal to cell walls, yielded stable thin foils of the same thin sections and microfossils as investigated by OM, AFM and SEM. Unicells that appeared excellently preserved by optical microscopy standards, consisted of disconnected kerogen particles, dispersed in the cryptocrystalline quartz matrix and arranged in stacks of variable spacing on micro- to nanometer scale. The density of carbon particles was found to be correlative to the stability of cell walls and to inhomogeneities in the chert. SEM and AFM images of cell cross-sections are directly comparable at the same scale of magnification, but AFM offers higher resolution possibilities and 3-D information on the arrangement of particulate carbon within the cell. Whereas the microscopic appearance of cells was highly variable within the same rock unit, from the same locality in the Chichkan Formation, the nanoscopic structure of kerogen was found to be similar in all cells, consisting of multi-laminated

* Corresponding author. Present address: Geology, Geo- and Environmental Sciences, Luisenstr. 37, D-80333 Munich, Germany. Tel.: +49 89 2180 6552; fax: +49 89 2180 6514.

E-mail addresses: mail@sciencepr.de (A. Kempe), wlady.altermann@iaag.geo.uni-muenchen.de (W. Altermann).

¹ Fax: +49 89 2180 4334.

(sheeted) amorphous carbon films, built up of layers with measured thickness between 10 and 20 nm, as revealed by TEM and AFM.

© 2005 Elsevier B.V. All rights reserved.

Keywords: Atomic force microscopy (AFM); Transmission electron microscopy (TEM); Focussed Ion Beam (FIB); Scanning electron microscopy (SEM); Acritarchs; Precambrian microfossils; Petrification; Microfossil micro-structure

1. Introduction

In paleontology, the micro-structure of fossil tissues has frequently been used for the characterization of organisms, transmission electron microscopy (TEM) being the prominent tool for viewing objects in cross-section on the nanometer scale. For the preparation of an ultra thin section of a cell, the carbonaceous material is usually isolated by chemical dissolution of the rock matrix, and extraction of the organic residue (Hemsley and Glasspool, 1999; Jones and Rowe, 1999a; Loeblich, 1970; Loeblich and Drugg, 1968; Loeblich and Tappan, 1969, 1971; Talyzina, 2000; Talyzina and Moczydlowska, 2000; Talyzina et al., 2000; Wellman and Axe, 1999; Yang et al., 1998). Large fossils, like plant leaves, can directly be grasped and treated as a whole (Jones and Rowe, 1999b; Osborn et al., 2000; Taylor, 1999), whereas small objects like microbes or pollen and spores have to be embedded in a solid resin before thinning (Jones and Rowe, 1999c). For example, in carbonates and cherts the palynomorphs and unicells are usually isolated by maceration of the rock, then sieved or concentrated by centrifugation (Williamson et al., 1999) and thus, removed from their original site of preservation and separated from the large portion of organic residue. This separation, due to technical necessities in preparation for TEM, causes a significant loss of information and is a potential source of contamination. In palynology, it would be most desirable to study pollen in the context of the associated plant (Guignard et al., 1998; Harley, 1997) and in the study of microbial life single celled organisms are preferably analyzed integratively within the context of the hosting stromatolite structure and the preserved paleobiocoenosis.

Another critical obstacle in fossil preparation is the poor preservation, especially of Precambrian microfossils. Even cells that appear well preserved and show rich detail under the optical microscope usually do not possess a contiguous wall structure on the microm-

eter scale (Kempe, 2003). Cell walls are often damaged beyond recognition by diagenetic processes. This makes very old fossils difficult to recognize unambiguously and has led to controversy on the authenticity of the world's oldest fossils (Brasier et al., 2002; Kazmierczak and Kremer, 2002; Schopf, 1993, 2004; Schopf et al., 2002a). Because of the discontinuous preservation, Precambrian microfossils tend to fall apart when the supporting quartz matrix is dissolved. Many objects that are well preserved by Precambrian standards were thus excluded from close examination by TEM in the past. A new integrative preparation must therefore create a stable section of the organic fossil within its mineralic host, in order to allow detailed investigation of the kerogenous remnants and their relationship to the embedding rock matrix.

Yet another constraint for a new preparation method, besides integrativeness and stability, is the possibility of applying several different methods of morphological analysis to the same specimen at all scales of observation. This is absolute prerequisite for a nanoscale study of poorly preserved microbes by scanning electron microscopy (SEM) or atomic force microscopy (AFM) (e.g. House et al., 2000; Kazmierczak and Altermann, 2002; Kempe et al., 2002; Kudryavtsev et al., 2000), because the examination of carbonaceous fragments at high resolution needs to be based on a reliable identification of the biological structures. In Precambrian micropaleontology, fossil recognition is mainly achieved by optical microscopy and statistically representative morphological description, being the most important method that allows for the assertion of the fossil and embedding rock relationships (Buick, 1991; Schopf, 1992a; Altermann, 2001). Three informal classes equivalent to the biological classes of prokaryotic filaments, prokaryotic coccoids and eukaryotic cells have been established (Schopf, 1992a,b), based chiefly on inspection of cells under the optical microscope. At least 279 taxonomic informal species of the Precambrian are known, based on

close similarities to extant unicellular organisms. Quality of preservation ranges from very thick, dark brown and black, contiguous carbonaceous fossil walls that are often multi-layered and show internal structure, to faint shades of carbonaceous material that represent the ‘ghosts’ of destroyed and mineral-replaced fossil walls.

In this paper, we present new methods for the analysis of fossil unicells on the nanometer scale, within their original embedding rock context, suitable for a combined study with optical microscopy (OM), Raman spectroscopy, SEM, AFM and TEM. We have applied Focussed Ion Beam (FIB) preparation to chert-permineralized Precambrian acritarchs, producing a $\sim 8 \mu\text{m} \times 20 \mu\text{m} \times 100 \text{nm}$ rock foil containing a section of the fossil wall for TEM imaging, directly from an optical thin section. After the extraction of the foil, the fossil unicell is still left in the original embedding rock in the thin section. A similar approach has been used by Schopf and Oehler (1976) and Oehler (1977), but seems to have been discarded. The method, allows for direct comparison of the results of different techniques, applied to the very same individual microfossil.

2. Materials and methods

2.1. Specimens

The fossil acritarchs (leiospheres) studied here are permineralized in carbonaceous cherty stromatolites (*Conophyton gaubiza*) of the ~ 650 Ma old Chichkan Formation from the Maly Karatau Mountains, Ayusakan, of southern Kazakhstan (PPRG Sample #1473; Moore and Schopf, 1992). Several hundred individual fossils were located by optical microscope in paleontological thin sections ($\sim 150 \mu\text{m}$ thick), cemented onto glass slides by acetone-soluble cement. Intact, relatively thick-walled, well-preserved spheroidal acritarchs $>30 \mu\text{m}$ in diameter, representing about 2% of detected fossils, were selected for further study.

2.2. Preparation

2.2.1. Preparation for AFM

Fossil-containing areas were demarcated by 3-mm-diameter circles drilled into the thin section surface (Sonatron sonic disintegrator drill, Kenyon Electron-

ics, Jersey City, NJ, USA); $\sim 1 \text{cm} \times 1 \text{cm}$ rectangles enclosing the circled areas were cut from the sections; the cementing medium underlying these rectangles was dissolved in acetone; and the fossil-bearing rock slices were re-cemented onto microscope slides. Individual microscopic fossils, situated close to the uppermost surfaces of paleontological thin sections, $\sim 300 \mu\text{m}$ thick, were located and photographed in transmitted white light with a digital video camera connected to a Zeiss Axiovert inverted microscope, then marked on the back side of the glass carrier with a diamond scribe. In a careful step-by-step process, controlled under an optical microscope, the section surface was then hand-ground with corundum powder and water on a glass plate, eroding roughly half the fossil and exposing the carbonaceous material of the cell walls on the surface of the section (Fig. 1A). Surfaces were hand polished with diamond powder and ethanol lubricant on a swivel disc, in successive steps with decreasing grain sizes of 6, 3, 1 and $0.5 \mu\text{m}$, in order to reduce irregularities in the rock surface to a minimum. Thus, later chemical preparation of the section surface was dependent only on the material contrast of the quartz in the rock and the kerogen in cell walls. The sections were submerged for 20–50 min in fluid HF 5% with the surfaces upside-down so as to let detached particles sink to the bottom of the acid bath. An optimum exposure time of 30 min could be verified for most fossils. Cells were photographed in reflected white light with the above-mentioned optical system, acquiring search-maps and reference images for AFM data. Subsequently, AFM studies of the surface structure were conducted.

2.2.2. Preparation for SEM and TEM

After AFM examination, specimens were first sputter-coated with a very thin gold layer that served as a trace line of the etched surface structure. The thin section was then coated with carbon for SEM imaging and to avoid charging of the specimen under the ion beam. TEM foil preparation occurred in a focused ion beam device by a Ga-ion beam accelerated to 30 kV. Preparation of ultra-thin foils by FIB is controlled by secondary electron imaging in the preparation chamber. For this application, the fossil wall must be exposed at the surface of the thin section and marked. The precise location for cutting a TEM foil across the cell wall was determined by comparing the previously acquired AFM image with the SE image obtained in the FIB. The

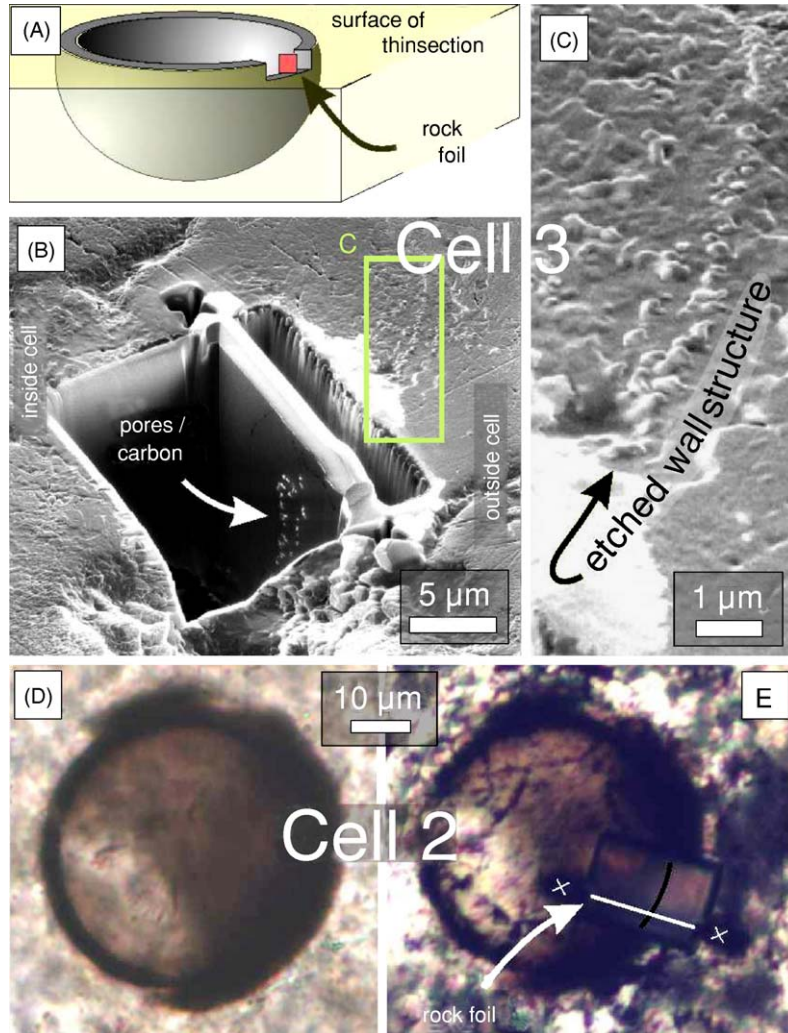


Fig. 1. Preparation of cell walls for AFM and TEM. (A) Sketch of a fossil cell with exposed surface after grinding and etching; the red part of the fossil wall represents the location of a TEM foil that was cut normal to cell wall. (B) SE image of a FIB prepared TEM foil typical for cell 3, before extraction from the thin section. The double wall structure appears as an etched prominence on the section surface (box) and as rows of bright pores along the rim of the cell visible in the foil. (C) Magnified SEM image of the boxed area in B. (D) Optical micrograph of cell 2 before FIB preparation. (E) Optical micrograph of cell 2 after FIB preparation; positions of removed cell wall (black) and TEM foil (white) are indicated graphically.

oil-free vacuum system of the FIB guarantees that the specimen will not be contaminated by carbon during the preparation process. The surface of the foil needs to be protected from being sputtered by the ion beam by depositing a thin Pt-layer on top of the surface. Pt-deposition occurs by decomposing an organic Pt-gas in the ion beam. Details of the FIB milling process are given in Wirth (2004) and references therein. The

TEM ready foil measures 15–20 μm by up to 10 μm and is about 150 nm thick. The foil is cut free at its base and on both sides. It is lifted out of the excavation site using an optical microscope. A glass fiber is attached to the foil as a special manipulator. Adhesive forces will keep the foil at the fiber's tip, so that it can be lifted and placed onto a TEM grid with a perforated carbon film as support for the foil. No further carbon

coating of the specimen is required. A final control of the cutting position and location of the TEM foil was achieved by optical microscopy in transmitted light. Cell 2 is shown before FIB preparation in Fig. 1D and after the TEM foil has been extracted in Fig. 1E, where the former location of the cell wall and the position of the TEM foil are highlighted.

The perforated polymer film on the TEM copper grid is electron transparent but gives rise to a weak mass absorption contrast, which is superimposed on the contrast of the object under investigation. However, the supporting film is perforated, which always allows to find regions where the sample is not overlapped by the film.

2.2.3. Preparation for OM

Because thick paleontological sections limit petrographic microscopy, some selected specimens were prepared for petrographic investigations, subsequently to AFM and SEM investigations. In order to turn the thick sections into petrographic (30 μm) thin sections, the sections were glued with the rock surface on another glass carrier, with acetone resistant glue. To avoid sticking of the old glass carriers to the new glass carriers, the old ones were covered with a thin coat of Vaseline.

After 24 h drying time, the rock sections, now sandwiched between the old and new glass carriers, were dipped in acetone to remove the old glass carriers, after a few minutes. Thereafter, the sections were ground down manually on a glass plate, with 800 corundum powder and under constant microscopic control of the thickness. In sections processed in this way, marking by pen was avoided, because under acetone the ink penetrates and soaks into the rock and cannot be removed completely from the rock surface, obliterating the microfossils. To facilitate the observation during grinding, the fossil location was marked by a diamond mark on the reverse side of the new glass carriers.

2.3. Raman spectroscopy

Prior to study by AFM, all fossils were analyzed by Raman spectroscopy using procedures of Kudryavtsev et al. (2000) and Schopf et al. (2002b). The laser-Raman spectra presented in Fig. 3 were obtained by the Dilor XY (formerly, Instruments S.A.; now JY Horiba) 0.8 m triple-stage system with macro-Raman, micro-

Raman, and line-scan Raman imaging capabilities. All three gratings of the system (each having a groove density of 1200 grooves mm^{-1}) were holographic, and the spectrograph was typically set in a subtractive configuration. Due to the confocal capability of the system, use of a 100 \times objective (having an extended working distance of 3.4 mm, a numerical aperture of 0.8, and not requiring immersion oil) provided a planar resolution of <1 μm and, by use of a confocal hole size of 150–200 μm , a vertical resolution of 1–3 μm . A coherent krypton ion laser equipped with appropriate optics provided laser wavelengths ranging from blue to infrared, of which 476 nm was used here to acquire spectra centered at 1400 cm^{-1} and extending from 800 to 1960 cm^{-1} . The typical laser power was <8 mW over a \sim 1 μm spot, an instrumental configuration well below the threshold resulting in radiation damage to fossil specimens such as those analyzed (Schopf et al., 2002b). Spectra of the carbonaceous walls of acritarchs were acquired from chert-embedded specimens situated <10 μm beneath the surface of a thin section and centered in the path of the laser beam projected through an Olympus BX40 microscope. To enhance the optical image of specimens in unpolished thin sections, the area analyzed was covered by a thin veneer (\sim 1 μm thick) of Type B non-drying microscopy immersion oil (R.P. Cargille Laboratories Inc.), the presence of which has been shown to have no appreciable effect on the Raman spectra acquired (Schopf et al., 2002b). All spectra shown (Fig. 3) are normalized to the corresponding spectral response function of the system. No evidence of the effects of polarization was detected in the spectra of any of the specimens analyzed.

2.4. Atomic force microscopy

The surface structure of etched fossils was measured by use of a Topometrix 'Explorer' AFM (Veeco, Mannheim, Germany) which is equipped with a 3-piezo scanner having a maximum planar range of 130 μm in each of the planar (x , y) directions and a maximum vertical (z) range of 10.5 μm , mounted on the video camera-connected inverse microscope. The images were acquired at a digital resolution of 300 pixels per line in each image, applying the intermittent contact mode (using NCHRW-reflex-coated and SSS-NCH cantilevers from Nanosensors, Neuchatel, Switzerland), selected among various scanning modes

tested as resulting in the least disruption of the scanned surface.

The surface structure of Cell 2 (Fig. 6F) was imaged with a ‘Dimension’ (Veeco) closed loop AFM in tappingTM mode, at a digital resolution of 512 lines per image and 1024 pixels per line, using Nanosensors’ SSS-NCH cantilevers.

2.5. Transmission electron microscopy

TEM was performed in a Philips ‘CM200’ transmission electron microscope operating at 200 kV and equipped with a LaB₆ electron source. The TEM is equipped with a Gatan Imagin Filter GIFTM and allows energy filtered imaging. Plasmon imaging using elastically scattered electrons applying a 20 eV window to the plasmon peak in the electron energy loss spectrum (EELS) allows discrimination between holes in the specimen and areas with very small sample thickness. In both cases in TEM bright field images, a very bright contrast would be visible. However, in plasmon images holes appear black, because in vacuum no electrons from the primary beam are scattered inelastically.

The carbon concentration in the TEM foils was analyzed by analytical electron microscopy (AEM) using the C–K X-ray fluorescence. The same signal can be used for carbon element mapping. AEM was performed with an EDAX X-ray analyzer. The spot size was about 4 nm and the dwell-time for each position was 45 ms. For the acquisition of an elemental map, a window with a certain energy range is selected, which includes the X-ray fluorescence line of interest. The integrated area selected by the window defines the signal used for mapping. This signifies that, even if there is no signal except for the background intensity, this background intensity will create a weak signal during the mapping. Consequently, the elemental maps always exhibit a weak background distribution of the selected element, which does not reflect the real distribution of the element but the intensity from the background. Additional elemental maps were acquired by electron energy loss spectroscopy (EELS) (three window method and/or jump ratio imaging) using the C–K edge (Fig. 7B).

SEM and point spectroscopy of the carbon concentration on the etched surface on the petrographic thin sections was performed with a Hitachi Cold Cathode Field Emission microscope that is equipped with an

Oxford Instruments EDX spectrometer, with a spatial resolution of $\sim 1 \mu\text{m}^3$.

3. Results

3.1. Preservation

Optical microscopy revealed that all cells selected for investigation were generally well preserved by optical standards, with the organic carbon in the cell bodies of dark yellow to brown color and in most cases appearing as continuous structures (Fig. 2). Nevertheless, cells displayed various degrees of detail-preservation: Some of the acritarchs are slightly deflated and have thick, but diffuse walls. Others are perfectly round. An exceptionally large and well-preserved example of an acritarch, with a thick wall is shown in petrographic thin section in Fig. 2. It has a clear, dark brown cell wall with brown halo inside and a narrower radiance zone outside the cell. The cell center is very clear. The cell is located at the edge of a very fine chert nest, rich in carbon. Within the cell, however, quartz crystallites are rather large, 10–20 μm across and of flame chalcedony type, with sharp boundaries (Fig. 2B).

Details of the cell wall are visible in a digital blow-up in Fig. 2C and D. The cell wall has indistinct, slightly diffuse boundaries. Many small “pearl-chain”-like, regular, carbonaceous structures are located on the inner cell wall and protrude into the cell or are arranged parallel with the cell wall. At different depths of focus the spheroidal nature of the single elements of the chains, arranged in clusters, is visible (arrows in Fig. 2E). These structures were only observed in petrographic thin sections of 30 μm thickness, where light refraction is low enough for good optical images. Carbonaceous chains are $\sim 1 \mu\text{m}$ in diameter and up to about 10 μm long and the spheroidal elements are below 1 μm in diameter, arranged in clusters of about 5 μm , and coating the inner wall of the cell with a regular, honeycomb-like layer.

Some cells studied are preserved at the edge of a very finely crystalline chert, within a transition zone to a somewhat coarser chert (c. 1 μm). Most of the sections are of equant quartz (equally large, mosaic textured recrystallized chert) of about 10 μm crystallite size, with sharp crystal boundaries. Only smaller patches are preserved as fine chert, mostly in the fossil

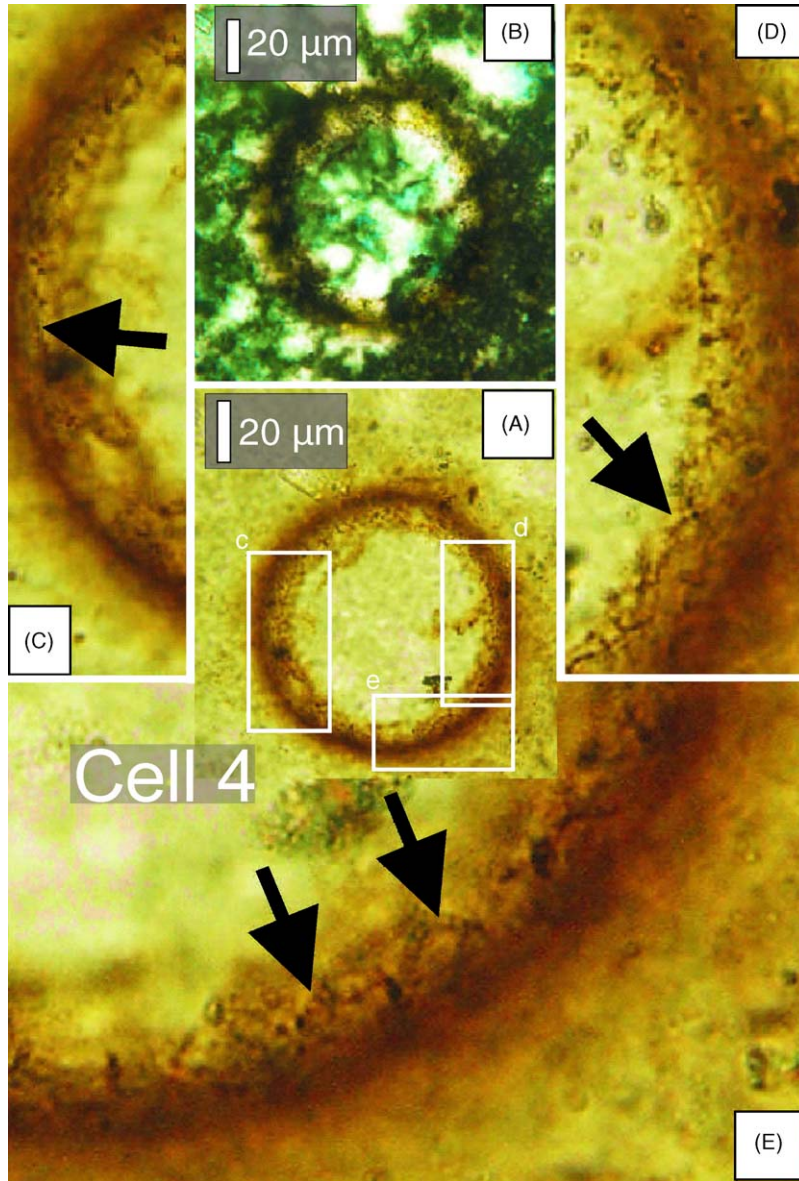


Fig. 2. Acritarch cell 4 in a petrographic, 30 μm thin section. (A) Cross-section through the cell displaying a relatively sharp, distinct cell wall (depending on the depth of focus) and a halo of kerogen inside and outside the cell wall. (B) The same cell under crossed Nichols, showing extinction properties of the cell-permineralizing quartz. In the lower right corner the chert is very finely crystalline. The other parts of the image display a coarser, recrystallized chert and a network of fine crystallites along the coarse quartz grain boundaries, where kerogen is concentrated as well. The cell wall itself is permineralized by finely crystalline chert, but coarser chert crystals penetrate it from the outside and chalcedonic quartz fills the cell interior, protruding into the inner kerogenous halo. (C–E) digital blow-ups of the cell wall parts as indicated by rectangles in (A), but taken at varying depths of focus. In (C) and (D) (arrows), the pearl-like chains of kerogenous, spheroidal structures are clearly visible. In (E), strings of such spheroids (arrows) and honeycomb-like clusters (in the background) are clearly discernible. Such preservational details within the embedding rock are only visible by optical microscopy as SEM and AFM measure only the surface of the sample, and TEM has not enough penetration potential and transmits only nanometer-thick samples.

vicinity and in areas where kerogen is concentrated. Within most cells, like in the example described above (Fig. 2), the crystal size was found to be markedly larger, recrystallized to above 1–5 μm , than within and outside the cell walls, where it is below 1 μm , if not recrystallized. In some cells, the center is filled with equant, recrystallized flame chalcedony. Carbon is not clearly discernable in the walls by optical microscopy, because its particles are below the resolution ability of the lens. Cells often also appear to contain Fe oxides or hydroxides.

TEM investigations in the direct vicinity of the wall structures and enclosing sheath confirmed the difference in grain size of quartz grains inside and outside the cells, being especially distinct where the carbonaceous fossil wall was more intact. It also showed that fine grains are typically linked to a high porosity of the chert, which was found to be especially dominant in a $\sim 5 \mu\text{m}$ wide margin around the cell wall. A typical example of this type of differential mineralization is presented in Fig. 5A, where the SiO_2 -filling of cell 1 consists of larger polycrystalline quartz with diffraction contrasts visible (dark bands in the grains). The chert outside the carbonaceous cell wall is composed of nano- to microcrystalline quartz grains that are riddled with cavities and organic carbon. The same differentiation was less pronounced in cells with a less intact wall structure (e.g. cell 2, Fig. 6A) and totally absent in poorly preserved fossils, as in cell 3 where a persistent nano- to microcrystalline quartz texture permeates the thin wall. Fig. 7 displays this type of homogeneous permineralization with quartz grains of different diffraction contrast, due to random orientation of the grains.

The kerogen throughout the sections displays a patchy distribution and is very fine, mostly far below the resolution ability of the optical microscope (below 0.1 μm), giving the sections a dark brown and pale brown diffuse appearance. Small, rare ghosts of a rhombic mineral (dolomite?) replaced by silica are present in parts of some sections. Rare cubic mineral ghosts could represent former diagenetic evaporite minerals, now thoroughly silicified. Several cells have inclusions within the cell interior. Some are fluid inclusions in quartz (pale and transparent) and some mineral inclusions, Fe-rich and dark. Some cells display a distinct halo of kerogen around them, which can be up to about 50% of the width of the cell, but clearly does not con-

stitute the cell wall. Where recrystallization is more advanced, this kerogenous brown “fog” is pushed away along the crystallization front and the quartz is clear, while the kerogen is concentrated along, and coats or wraps around quartz crystal boundaries. The chert is clearly finest where richest in kerogen.

3.2. Stability/integrity of cell walls

For 32 analyzed specimens of acritarchs from the same rock unit and locality in the Chichkan Formation, three different grades of preservation ranging from intact to semi-intact, to disrupted, were defined. Best preservation was represented by cells with intact carbonaceous cellular structures and high chemical resistance to hydrofluoric acid, poorest preservation by cellular structures which were non-contiguous on the micrometer scale and very unstable upon HF exposure. Three typical unicells with an organic double wall structure of declining grade of stability upon HF-exposure are presented in Figs. 5–7; best preservation being represented by cell 1 (Fig. 5) which shows a distinct complete cell wall, poor preservation being represented by cell 3 (Fig. 7) displaying a very thin interrupted wall structure, and intermediate preservation in cell 2 (Fig. 6), where the semi-contiguous wall showed only small gaps, filled by quartz crystals. TEM foils transecting the cell walls of all qualities of preservation could be acquired without exception by the FIB technique.

3.3. Carbonaceous structure on micrometer scale

Raman spectra of the kerogenous cell walls of each of the 32 acritarchs studied were acquired from chert-embedded specimens analyzed in situ. Typical spectra are shown in Fig. 3, acquired from each of the specimens illustrated here (Figs. 1, 2, 5–7). The two most prominent features of the Raman spectra of the fossils analyzed are a band of high intensity at $\sim 1600 \text{ cm}^{-1}$ and a group of bands centered at $1300\text{--}1350 \text{ cm}^{-1}$ (Fig. 3). Both of these spectral features are characteristic of the carefully studied and well-documented Raman spectra of polycyclic aromatic hydrocarbons, “PAH’s” (Mapelli et al., 1999a, 1999b; Rigolio et al., 2001; Castiglioni et al., 2001a, 2001b; Negri et al., 2002). In such spectra, the most intense Raman band, at $\sim 1600 \text{ cm}^{-1}$, is ascribed to synchronous aromatic ring

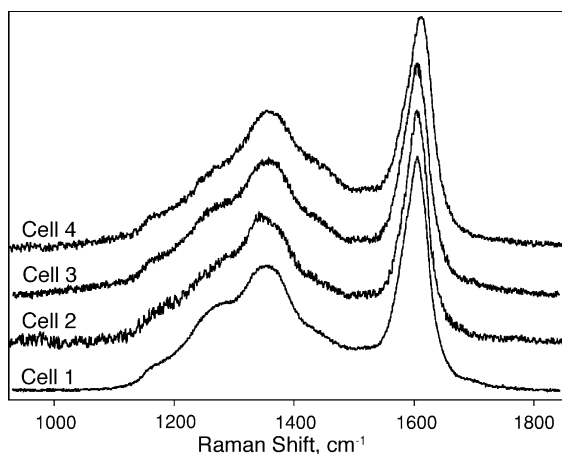


Fig. 3. Raman spectra taken from the walls of individual cells 1–4.

stretching whereas the bands in the 1200–1400 cm^{-1} range are attributed to modes of aromatic ring deformation and totally symmetric breathing (Mapelli et al., 1999b). The spectra acquired from the Chichkan acritarchs (Fig. 3) are thus consistent with a large body of data establishing that fossil kerogens are composed predominantly of more or less regularly stacked arrays of interlinked PAH's (Durand et al., 1977; Durand, 1980; Faulon et al., 1989; van Krevelen, 1993; Vandebroucke, 2003). More detailed Raman analyses show the geochemically moderately mature Chichkan kerogen to be exceptionally little altered in comparison with the kerogenous components of more than a score of other fossiliferous Precambrian deposits (Schopf et al., 2005).

The carbonaceous wall structures exposed on the rock surface by HF-etching were imaged with AFM, later combined with SEM/EDX analysis. On the petrographic thin sections, elemental mapping for C, Si and Fe was performed. Fe mapping revealed very low-Fe presence, not reflecting the shape of the cell, but only an irregular, patchy Fe distribution. Also the attempt to map for Al, Mg, Ca and K did not reveal any element distribution patterns related to cell morphology. Obviously carbonates, phyllosilicates and feldspar do not play any role in the fossilization process of these cells. It appears, however, that Ca and Mg slightly reflect some recrystallization shapes of quartz.

In all cases of C-mapping, the area maps showed a distribution correlating with the shape of the preserved cell or with the SiO_2 crystallite along the cell wall.

The same can be seen, but less clearly, in Si distribution maps, where C substitutes for Si. From the point spectra taken on elevated structures within the cell wall and on elevated particles in the direct outer vicinity of the cell wall (comp. Fig. 6G), it can be seen that the C-peak is relatively low in comparison to the Si-peak (and O-peak). However, with increased resolution and magnification, in spot measurements, the C-peak rises significantly. Spot mapping thus confirmed that the parts of the cell wall that form elevated structures after HF preparation consist of carbon.

Although all of the 32 specimens possessed an organic wall, that was optically coherent over large stretches, only 9 showed fossil walls that were stable at acid exposure. In very well preserved cells (dark under optical microscope and of dense carbon distribution in TEM section) HF-etching produced walls rising 200 nm above the rock surface that could be imaged with the AFM already after 20 min of acid exposure. These cell walls grew as high as ~ 1000 nm after 30–40 min of exposure (e.g. Fig. 4K and L). Longer etching times of up to 70 min resulted in 2000 nm high cell walls and large cavities in the centers of the cells, where pure quartz, recrystallised after flame chalcedony, was present. Large holes proved to be very inconvenient for AFM imaging, thus defining the upper limit of etching time. Optically thin-walled fossils showed less differential etching contrast, producing a flat relief that was best detectable by AFM when the polished surface was only slightly eroded by etching (e.g. Fig. 7G and H). After more than 30 min etching, the whole structure became increasingly degraded so that material difference became unrecognizable.

The different grades of stability versus HF-etching were documented by AFM in the three examples of

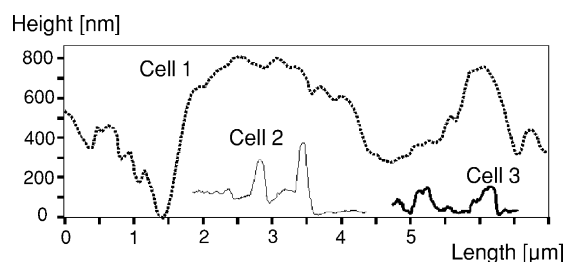


Fig. 4. Topography of fossil walls after 20 min HF-exposure, measured by AFM. Positions of the corresponding transects are indicated by blue lines in Figs. 5L, 6F and 7H.

cells 1–3. Fig. 4 displays profiles through the etched walls of cells 1–3 (along the blue trajectories in Figs. 5L, 6F and 7H), after 20 min of etching, showing that good quality of preservation corresponds to tall wall structures in cell 1, with lower topography in cells 2 and 3.

Along with height, the compactness of the fossil structures increased with preservation quality. In the AFM images of cell 1 (Fig. 5K and L), a very solid uninterrupted fossil wall prevails in about half the circumference of the whole cell, the inner wall being much more pronounced than the outer structure. Cell

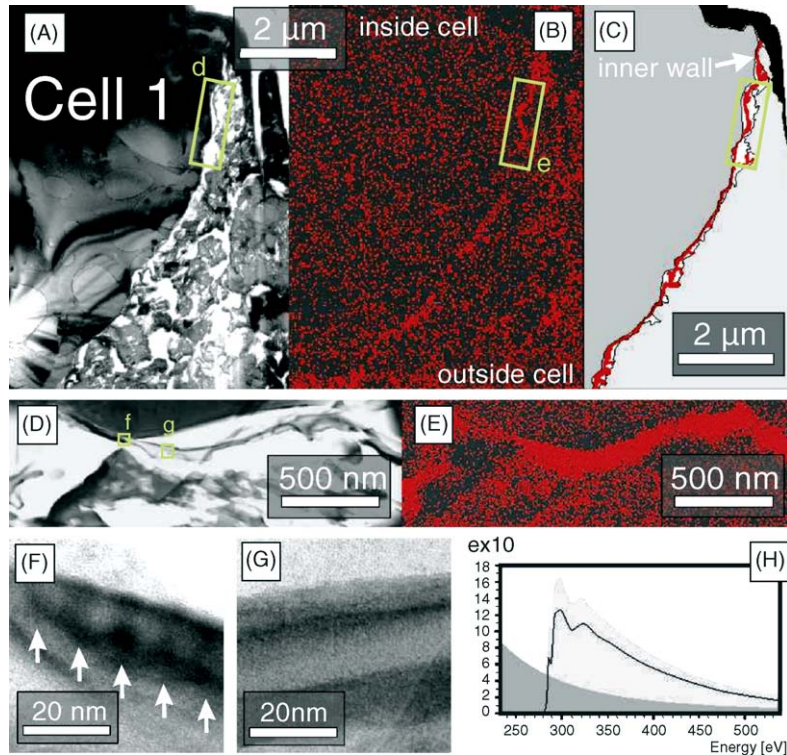


Fig. 5. Structural analysis of cell 1. (A) TEM bright field image of a part of the TEM foil cut normal to the cell wall. Bright to nearly white areas represent holes in the foil or very thin carbon layer. The uniform dark grey contrasting material in the left part of the image represents coarse-grained quartz. The patchy-appearing contrast in the right part of the image is due to fine-grained quartz (darker grey or black), amorphous carbon (light grey) and holes (white). (B) C-elemental map (EDX), corresponding to (A). It shows an increased amount of carbon along the boundary of the coarse-grained quartz and the fine-grained quartz. (C) Sketch of the main components in the carbonaceous structure along the fossil boundary shown in (A) and (B). Coarse SiO₂ in dark grey and fine SiO₂ in light grey, C_{org.} in red, Pt-cover on surface from FIB preparation in black. (D) TEM bright field image of the area indicated by a box in (A), showing a wavy, string-like dark grey film, built up of amorphous carbon, and adhering to the overhead quartz grain at label f and spanning over the vacuum at label g. (E) EDX, Carbon map corresponding to (D). (F) Energy filtered plasmon image from the area labeled f in (D); this section of the film shows a substructure, with regular spacing, entirely consisting of amorphous carbon. (G) Plasmon image from the area labeled g in (D). The image shows a three-layer structure in the amorphous carbon material. (H) Electron energy loss spectrum representative for all carbonaceous structures analyzed; original spectrum in grey; background fit in dark grey; spectrum after subtraction of background as black line. (I) Optical photomicrograph of a well-preserved cell, showing high concentration of carbon in the center and along the outer double wall structure, as indicated by the dark brown color. (J) True scale sketch of the fossil wall structure, superimposing the dark brown areas in (I), represented by the continuous line, with the etched relief in (K), represented by the dashed line. (K) AFM image of the leiosphere after 20 min etch with 5% HF, showing elevated structures at localities of high carbon concentration in the double wall and center. Image taken after erosion of ~1 μm of material from the surface. (L) AFM image of the boxed area in (K). The blue line indicates the transect through the cell wall along which the topographic profile shown in Fig. 4 was measured. (M) Magnified AFM image, corresponding to the box in (L), showing a 3-D view of stacks of carbonaceous components in the inner wall structure.

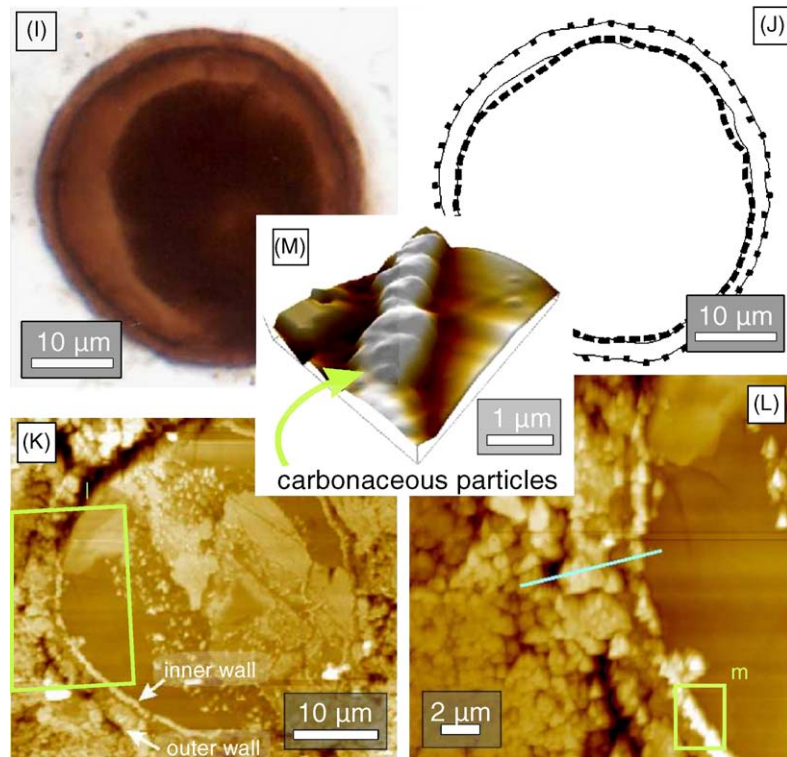


Fig. 5. (Continued).

2 displayed a less homogeneous carbonaceous wall, with spots of high elevation above the etched rock surface, e.g. the structure in the center of Fig. 6F, but less pronounced wall for most of its expansion. EDX spot analysis (Fig. 6G) demonstrated the carbonaceous nature of the elevated structures within the wall (green squares), as well as of those elevated structures dispersed in the embedding chert outside the cell, which envelop the inner cell wall within a 5 μm thick spherical margin. Cell 3 had the thinnest etched double wall structure of all cells, which appears as a stippled half circle in the upper portion of Fig. 7G. Higher magnified topographical maps (Fig. 7H and I) showed the non-continuous nature of this fossil wall.

TEM bright field imaging (Figs. 5A, 6A and 7A) displayed cavities and the carbonaceous content of the cells in light grey to white contrast, contrary to the dark grey contrast, typical for the micro- to nanocrystalline quartz matrix of the embedding rock. In approximation, all bright parts in the TEM images can thus be regarded

as portions of the fossil. Cell walls are well visible as round, approximately 1–3 μm thick structures. Elemental maps (Si–K, C–K) of the fossil walls showed that quartz components were interfusing the cell walls and comprised the major part of the whole fossil structures, so that carbonaceous cell walls were discontinuous in most cases. The walls of the acritarchs described here can thus be regarded as a quartz–kerogen composite or as kerogen disrupted by quartz crystallites. The carbon constituent of the composite showed generally sharp boundaries towards the inside of the cell and flame-chalcedony. Carbon constituent that reached 3–10 μm towards the outside of the cell, formed a less well-defined outer boundary. In the better-conserved cells, the innermost part of the fossil wall consisted of larger intact pieces of carbonaceous film, whereas the outward part hosted dissected fragments of such a carbon film. The same characteristic distribution of carbon has been described for eukaryotic unicells from the Bitter Springs Formation, also applying TEM studies of whole rock specimens (Oehler, 1977; Schopf and

Oehler, 1976), being interpreted as cell walls and cell sheaths.

Out of the three examples of TEM analysis shown here, only cell 1 has an intact inner cell wall, the outer wall and surrounding area comprise of discontinuous carbonaceous particles (Fig. 5A). The less well-preserved cell 2 displayed on a large scale, an almost coherent inner wall structure (Fig. 6A and B) and an exterior carbonaceous wall and carbon halo that is interfused by larger volumes of quartz. The single portions of the cell wall, viewed on a smaller scale

consist of flat carbon fragments, 1–3 μm in diameter, very closely spaced, aligned and interrupted by small volumes of quartz crystals. The cell wall carbon was thus non-coherent in cell 2. Fig. 6C–E depict single fragments of carbon, each surrounded and overlapping with crystalline quartz. In cell 3, all carbonaceous parts are separated by large volumes of quartz and the inner- and outer cell wall are indistinguishable (Fig. 7A).

The structure of the carbon particles comprising the cell walls was documented in detail in elemental maps

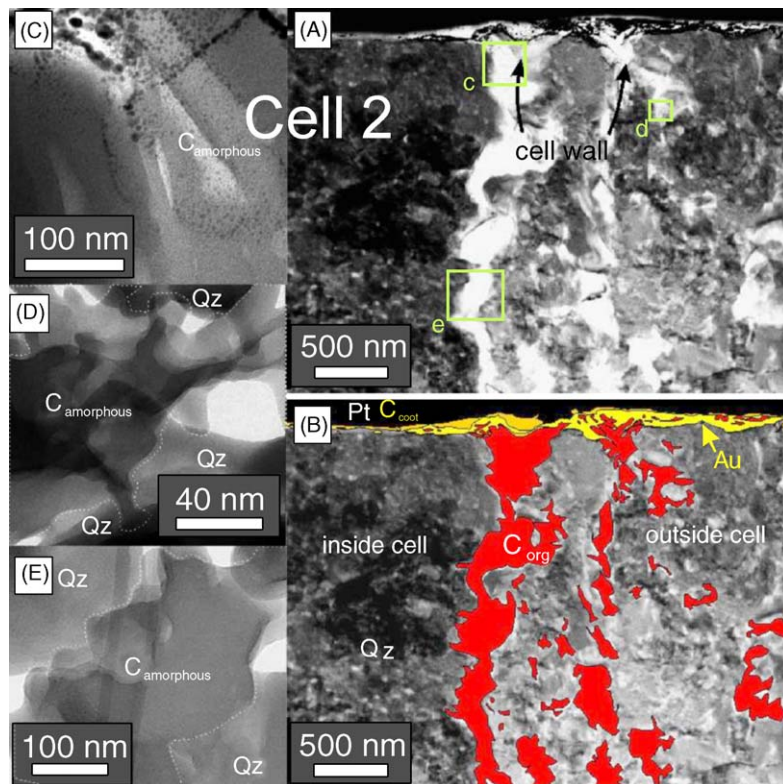


Fig. 6. Structural analysis of cell 2. (A) TEM bright field image of a part of the TEM foil cut normal to the cell wall. Bright or nearly white areas represent holes in the foil or very thin material. The patchy dark grey contrasting material in the image represents crystalline quartz. (B) Sketch of areas with accumulated carbon along the fossil boundary shown in (A); SiO_2 unmarked, C_{org} in red, Au-coat in yellow, C-coat in orange, Pt-coat in black. (C) Plasmon image from the area labeled c in (A), showing stacks of carbonaceous sheets in side view. (D) Plasmon image from the area labeled d in (A), showing stacks of carbonaceous sheets in plan view, embedded in quartz grains. (E) Plasmon image from the area labeled e in (A), showing stacks of carbonaceous sheets in plan view, embedded between quartz grains. (F) AFM image of the leiosphere after 20 min etch, showing revealed carbonaceous structures, where removal of quartz matrix has created depressions. Image taken after erosion of ~ 500 nm of material from the surface. The blue line indicates the transect through the cell wall along which the topographic profile shown in Fig. 4 was measured. (G) SEM image of that portion of the fossil wall labeled g in (F); EDX point spectrum, representative of all excavated structures shown in (F) (e.g. arrows); this spectrum was taken at the spot labeled with a green circle in (G) and (F). (H) AFM image in 3-D view of one carbonaceous platelet outside the cell, labeled h in (F).

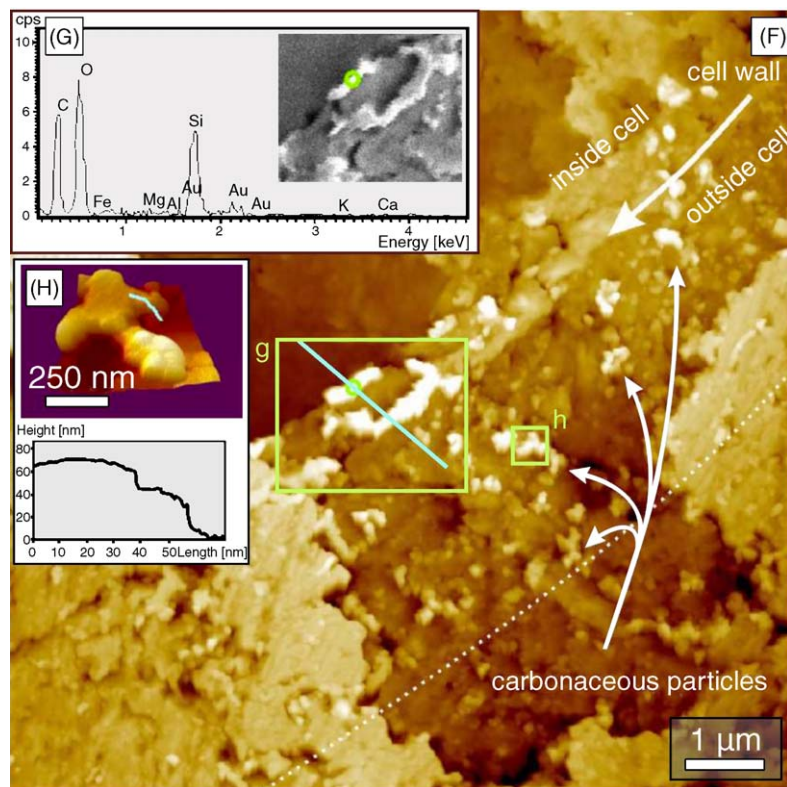


Fig. 6. (Continued).

obtained by EDX and EELS. In TEM, wall structures were best traced by carbon elemental mapping (EDX) in very well-conserved fossils, like cell 1. The EDX image in Fig. 5B displays a contiguous carbon structure within the quartz frame filling cell 1 and carbon enrichment in the proximal cavities outside the cell. A more precise assignment of carbon to the cellular structure with EDX was possible at higher magnification, as shown in the close-up mapping of one section of the inner cell wall, in Fig. 5D–E. Visualized at the nanometer scale, the carbonaceous wall appears as an ultra-thin film, adhering to quartz crystals of the cell-filling (top) and the embedding quartz matrix (bottom) in some places, but spans empty cavities in other parts (Fig. 5D). The carbon signal shown in Fig. 5E clearly maps the laminar structure. Elemental point spectra from the carbonaceous film and crystals were taken on multiple spots. In less well-preserved fossils, the carbon signal of smaller cellular fragments was dominated

by the background noise in large survey scans, but was visualized for smaller portions of cell wall at higher magnification. Figs. 7C–D shows fragments of carbonaceous film embedded in microcrystalline quartz framework.

As an overall result, carbon mapping confirms that carbon films are partly filling inter-granular cavities in the crystalline SiO_2 -matrix. EELS spectra acquired with a spot size of 55 nm show a C–K edge, characteristic for amorphous carbon. All carbon structures found were amorphous by identification with the established fingerprint technique (Garvie et al., 1984), which allows for discrimination between the phases of amorphous carbon, graphite and diamond. No crystalline carbon was found. Fig. 5H depicts a typical spectrum of such amorphous carbon. The light grey shaded spectrum is the raw spectrum. The dark grey-shaded spectrum is the modeled background and the black curve represents the background-subtracted spectrum.

3.4. Wall structure on nanometer scale

Whereas the structure of the entire cells was found to be of variable stability, completeness and coherence at all grades of preservation, the carbonaceous component of the fossil walls consisted of similar films of amorphous multi-sheeted carbon. These films are presented at nanometer resolution in TEM (EELS: Fig. 5F and G, Fig. 6C–E and as a plasmon image in Fig. 7B), where each additional carbon sheet increases the mass adsorption contrast in the image. Single fragments of C-film in cavities between the quartz crystals, in cells 2 and 3, showed various shapes and sizes, typical for amorphous sheeted carbon material.

Fig. 6C displays planar stacked carbon sheets of very regular, rectangular shape at the surface of the polished

and etched thin section. Fig. 6D shows a planar sheeted complex at a depth of $\sim 0.5 \mu\text{m}$ below the section surface, with amoebae-like forms that vary greatly in shape for each lamina and which overlap the neighboring quartz grains. Fig. 6E depicts a planar sheeted particle of compact, irregular shape at a depth of $\sim 2 \mu\text{m}$, also overlapping the surrounding quartz crystals.

In EELS images, the carbonaceous substance is difficult to discriminate from the very tiny quartz, and very thin carbon sheets are difficult to distinguish from vacuum, by the optical impression. Therefore, carbon was mapped in all EELS images and superimposed on the corresponding bright field images. The outlines of the carbonaceous material have been indicated by stippled lines in the bright field images in Fig. 6D and E. A clear distinction of quartz and carbon was made by

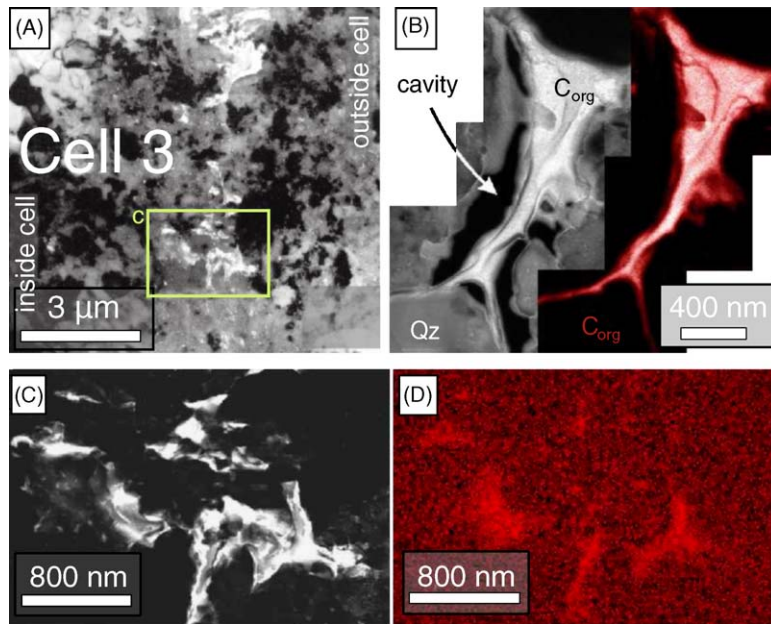


Fig. 7. Structural analysis of cell 3. (A) TEM bright field image from a foil cut normal to the cell wall. The bright areas indicate porous structures in quartz grains together with carbon-rich material. (B) The left portion of the image is an energy filtered TEM plasmon image applying a 20 eV window to the plasmon peak in the EELS spectrum; a carbonaceous multi-layered film is represented by light grey scales, crystalline quartz in dark grey and vacuum in black. The right portion of the image is the corresponding carbon elemental map (EELS), clearly identifying the central structure as carbonaceous. (C) TEM bright field image corresponding to the box labeled c in (A), exhibiting “pore”-space filled with amorphous carbon between quartz crystallites. (D) Elemental map (EDX) corresponding to (C). (E) Optical photomicrograph of the regularly preserved cell, showing high concentration of carbon along the outer double wall structure, as indicated by the dark brown color. (F) True scale sketch of the fossil wall structure, superimposing the dark brown areas in (E) (continuous line) with the etched relief in (G) (dashed line). (G) AFM image of the leiosphere after 20 min etch, showing very fine elevated structures at the localities of high carbon concentration in the double wall structure. Image taken after erosion of $\sim 200 \text{ nm}$ of material from the surface. (H) AFM image, corresponding to the box labeled h in (G). The blue line indicates the transect through the cell wall along which the topographic profile shown in Fig. 4 was measured. (I) Magnified AFM image, corresponding to the box in (H), showing a 3-D view of the carbonaceous components of the outer wall structure.

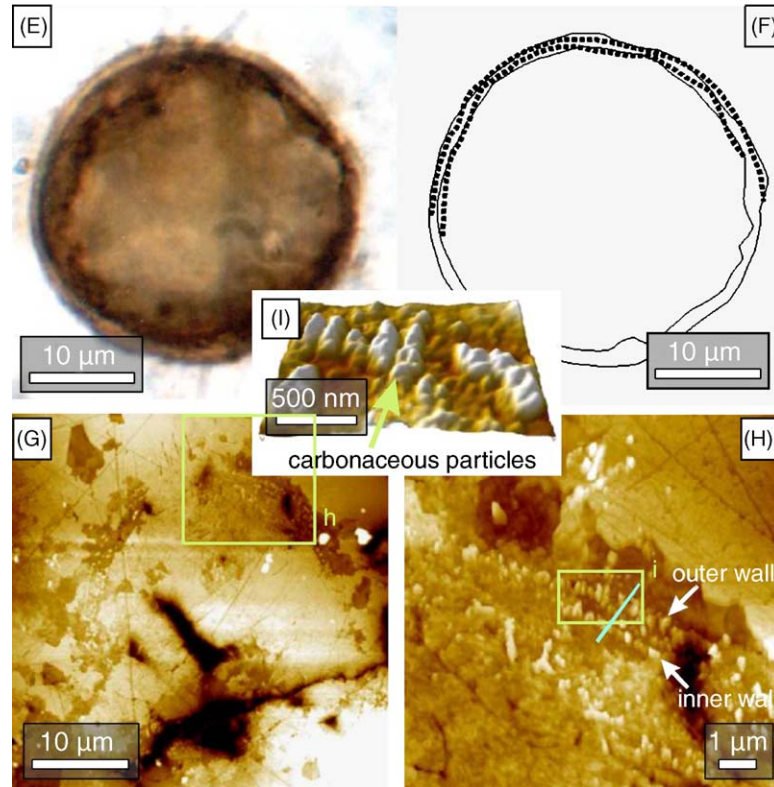


Fig. 7. (Continued).

carbon–K edge mapping presented in Fig. 7B, where the left portion of the figure is a plasmon mode image (energy filtered), in which crystalline quartz appears in dark grey, carbon in bright grey and vacuum in black. The right portion of the image is the corresponding carbon elemental map with the C–K edge intensity shown in red color. The images display a multi-layered piece of carbon film that wraps around quartz crystals, forming a bifurcation in its lower part, altogether appearing wrapped and folded.

The intact wall of cell 1 was imaged at nanometer resolution, displaying a carbonaceous film in cross-section (Fig. 5F and G). Also here, the C-film is sheeted, each lamina having a thickness of ~ 10 nm, which is an approximation since the structure is folded. Some internal structures with larger mass absorption contrast than in the surrounding film were found in one lamina (Fig. 5F). These structures are arranged perpendicular to the film surface, forming some sort of cross-channels or supports. The channels have a regular spacing of

~ 10 nm. The total width of the film in a section at its thinnest point is 30 nm.

For carbonaceous flakes that have been imaged in top view, like in Fig. 6E, the thickness of carbon sheets was calculated using the zero loss peak intensity (I_0) and the total spectrum (I_t). From total intensity of the spectrum (I_t) and the intensity of the zero loss peak (I_0) in the equation $t/\lambda = \ln(I_t/I_0)$, the ratio of specimen thickness (t) divided by the electron mean free path (λ) can be calculated (Malis et al., 1988; Egerton, 1989). The calculated electron mean free path, λ , for carbon at an acceleration voltage of 200 kV is about 150 nm. The resulting thickness for the multi-layered particle shown in Fig. 6E is 100 nm.

AFM analysis of the surface structure of fossil walls at nanometer resolution revealed sheeted carbon particles that were found in fossils of all qualities of preservation, but did not generally cover the whole wall structure. Fig. 5M displays a section of the wall of cell 1, where an array of stacked carbonaceous particles,

ranging from 100 nm × 400 nm to 400 nm × 1000 nm, prevails. Such an arrangement was also found in cell 3 (Fig. 7I). The size of these particles is comparable to the dimensions of the carbonaceous flakes visible in TEM section and has been evaluated statistically for all fossils (Kempe, 2003), showing distributions in thickness with peaks at ~20 and ~300 nm. The regularity in spacing, the size distribution and the three dimensional orientation patterns are striking. In the particular examples of cells 1 and 3, carbon particles seem to stand upright and parallel to the cell radius. However, the section through cell 2 showed carbonaceous particles in the wall and directly outside the wall, that were not regularly oriented. Most particles are lying flat in the substrate in this particular section of the cell, like the particle displayed in Fig. 6H, located within the sheathing margin of the cell. At this orientation, the particles are similar in shape when viewed in AFM and TEM.

The multi-sheeted carbon structure seen in transmission EM has been reported before (Kempe et al., 2002) and referred to as “platelet structure”. Fig. 6H shows a three dimensional view of a single carbonaceous particle (or platelet), imaged at a digital spatial resolution of 1 nm and an approximate physical spatial resolution of 3–5 nm. In the topographic profile, the same amoebae-like flat shape and the multi-layered composition that prevails in the TEM images is visualized. The step size of single carbonaceous layers was measured, and varied between 15 and 30 nm, as visualized in the height profile, corresponding to the pale blue line in Fig. 6H.

4. Summary and conclusions

AFM imaging of fossils in petrographic slides, combined with SEM and optical microscopy and the combination with TEM imaging of ultra thin foils, prepared from the same slides, provide information on the three dimensional structure and composition of fossils at the nanometer to micrometer scale and on the nature of fossilization of the cells. In combination with in situ micro-isotopic analysis (House et al., 2000) and molecular analysis of fossil remnants (Brocks et al., 1999), the methods introduced herein can help to definitely decide on the authenticity of the alleged microfossils.

In a study of 32 Precambrian spheroidal unicells that appeared as excellently preserved fossils under the optical microscope, only 10 cells showed considerable

resistance to hydrofluoric acid. All other cells tended to fall apart upon preparation, during mild and selective etching with HF. These 10 stable cells were imaged in section by atomic force microscopy. After etching, each fossil was protruding to a different degree from the surrounding rock surface and the cells that produced very stable high walls had a very solid, compact wall structure. Those cells with low walls consisted of loosely dispersed carbon particles embedded in and disrupted by quartz, crystallized during diagenesis and at later stages of the rock’s history.

Focussed ion beam preparation enabled us to examine microfossils of varying preservation quality, at the nanoscale under TEM and AFM. The method is particularly interesting for the study of Precambrian fossils, where poor preservation can cause a major difficulty in preparation of macerates and where taphonomic and preservation details are important for the judgement of the authenticity of the objects investigated. It is remarkable that the extraction of foils by the FIB technique was achieved without losses for very solid cell walls, as well as for the more fragile fossil walls. The enframing chert showed ideal sputtering characteristics so that flat, unwrapped foils with maximum sizes of 8 μm × 20 μm and a thickness of ~100 nm were produced for each cell, whereas etching of the petrographic slides produced walls that fell apart at a maximal wall height of ~2 μm. FIB thus proved to be an excellent tool for probing fossil unicells at precisely defined locations.

TEM examination of the thin foils showed that the carbonaceous cell structure consists of particles of amorphous carbon (kerogen) in the size range of 1–3 μm. Particles are dispersed in the chert rock at the original location of the cell walls and in their surroundings, and the carbon apparently wraps around nanometer to micrometer scaled quartz crystallites. The same can be observed by optical microscopy of petrographic thin sections, where the carbon has been pushed forward along the crystal boundaries, by the crystallization force of the growing quartz crystals, and wraps around such crystals which have a size between <1 and 5 μm. This behaviour bears a high risk for misinterpretation of such carbon wraps around quartz as unicells, when cherts are investigated for microfossils only by SEM. Such carbon wrapped quartz crystallites and carbon films embedding quartz, appear after mild etching as coccoidal, cucumber-shaped or short filamentous single cell-like structures and colony-like

assemblages, in a two dimensional surface investigated under the SEM. Various shapes mimicking dividing cells and cell colonies can be produced by etching of kerogenous chert or by simple breaking along weakness fractures, and easily be misinterpreted for microfossils, as discussed by [Altermann \(2001\)](#), especially as EDAX carbon mapping will show they carbon content without revealing they quartz crystallite nature. The best method to avoid such misinterpretation is previous thorough investigation of thin sections by optical microscopy and identification of microfossils within their rock content.

Whereas the structural constitution of cells as a whole was greatly variable within the individual stromatolites sampled, the nanoscale structure of kerogen was remarkably homogeneous. By analysis of Raman spectra, the fossil kerogen was found to show molecular similarity to interstellar dust as well as to quenched carbonaceous composites (QCC) and hydrogenated amorphous carbon (HAC), which all consist of islands of aromatic (sp^2) bonded C atoms joined together with a variety of peripheral sp^2 - and sp^3 -bonded hydrocarbons ([Kwok, 2004](#)). As in these three classes of carbonaceous material, electron micrography of the fossil kerogen showed a structure, varying from amorphous to electron diffractive.

In all fossil walls as well as in the intact wall in cell 1, the kerogen consisted of multi-layered, amorphous carbon film, or small fragments of such a film. The outer shape of particles varied within one fossil and from cell to cell, being angular or lobate, flat or wrapped, compact or spliced, but the multi-layered structure was always found to be laminated with an approximately regular lamina thickness. The thickness of the sheets could be measured directly in the cases where the foil preparation had produced a normal section through carbon sheets. Another possibility of calculating the thickness of single laminae is the evaluation of the energy loss spectrum on kerogen particles lying flat in the focal plain. Both methods yielded average thickness between 10 and 20 nm per carbon sheet. Sheets have also been imaged by AFM, yielding a thickness between 10 and 30 nm. These results are in good agreement with structural data published before ([Kempe et al., 2002](#)). The carbonaceous nature of the platelets then deduced by laser Raman spectroscopy ([Kempe et al., 2002](#)) has now been confirmed with TEM imaging, EDAX element mapping and spot analyses of

single components, of controlled (SEM, TEM, AFM) locations within the particular cell.

The three dimensional arrangement of kerogen particles within the cell walls was apparent in AFM topographical mapping. Here, flat particles or platelets, arranged in stacked arrays, in the manner of tiles, constitute solid cell walls. Stacks of carbon platelets appeared dense in those cases, where the spacing in TEM section was also found to be dense, and vice versa. However, the described stackings of carbon platelets were not continuous over entire cell walls and they were not found in all cells. These irregularities may be due to local variances in degradation processes (cell lysis) and to (post-) diagenetic alteration.

The spacing of carbon particles (platelets) was approximately regular within one fossil but varied greatly from one unicell to the other. Not surprisingly, those cells with the densest distributions of carbon in the fossil wall were also most resistant to acid exposure. Optically, we consider those fossils with dense, dark carbon to be well preserved. In this sense, cells 1–4 were ideally preserved, because they displayed a largely uninterrupted carbonaceous wall. However, TEM and AFM revealed the discontinuous nature of all but one fossil (all but cell 1), which corresponded to the varying grades of stability of the cell walls upon HF etching. This structural observation obviously must be used to redefine the term “preservation quality”.

The biological and taphonomic significance of the here described preservation is yet enigmatic. The morphology and size of the platelets and the internal structure of the carbon films, with sheeted lamina having a thickness of ~ 10 nm and with supports regularly spaced perpendicularly to the laminae, at ~ 10 nm distance, is certainly a function of combined processes of *post mortem* bacterial cell degradation and diagenesis, but mainly of the metamorphic history of the rock. Reorganization of the genuine cell material into polycyclic aromatic hydrocarbons has obviously taken place, the original biochemistry being destroyed. Most of the cell (wall) structures have been altered, resulting in the uniform multi-layered carbon films that consist of planar domains of interlinked planar aromatic makro-molecules, which are electron amorphous. The detected internal ultra structures in very well-preserved fossils reflect most likely recrystallization effects during late diagenesis and weak metamorphism. However, the detailed contribution of the

involved processes remains yet to be experimentally evaluated.

In summary, we conclude that AFM and TEM techniques combined with the Focussed Ion Beam preparation method and Laser Raman spectroscopy significantly support the investigations of Precambrian microfossils, adding new, up to now inaccessible information on the fossilization processes and on the nanoscopic structure of the fossils. However, optical microscopy remains an important and inevitable basic method in Precambrian micropaleontology, providing crucial information on the fossils and their relationship to the hosting rock.

Acknowledgements

Financial support through DAAD (Kempe, Heckl), NSF (Schopf) and Le STUDIUM (Altermann) is gratefully appreciated. Annie Richard, Department of Physics, University of Orléans, France helped with SEM and EDAX analyses; A.B. Kudryavtsev, University of Birmingham, Alabama, USA carried out Raman spectroscopic measurements. Pat Eriksson University Pretoria, critically read the manuscript.

References

- Altermann, W., 2001. The oldest fossils of Africa—a brief reappraisal of reports from the Archean. *J. Afr. Earth Sci.* 33, 427–436.
- Brasier, M.D., Green, O.R., Jephcoat, A.P., Klepepe, A.K., Van Kranendonk, M.J., Lindsay, J.F., Steele, A., Grassineau, N.V., 2002. Questioning the evidence for Earth's oldest fossils. *Nature* 416, 76–81.
- Brocks, J.J., Logan, G.A., Buick, R., Summons, R.E., 1999. Archean molecular fossils and the early rise of eukaryotes. *Science* 285, 1033–1036.
- Buick, R., 1991. Microfossil recognition in Archean rocks: an appraisal of spheroids and filaments from a 3500 My old chert-barite unit at North Pole, Western Australia. *Palaios* 5, 441–451.
- Castiglioni, C., Mapelli, C., Negri, F., Zerbi, G., 2001a. Origin of the D line in the Raman spectrum of graphite: a study based on Raman frequencies and intensities of polycyclic aromatic hydrocarbon molecules. *J. Chem. Phys.* 114, 963–974.
- Castiglioni, C., Negri, F., Rigolio, M., Zerbi, G., 2001b. Raman activation in disordered graphites of the A1' symmetry forbidden k0 phonon: the origin of the D line. *J. Chem. Phys.* 115, 3769–3778.
- Durand, B., Marchand, A., Amiell, J., Combaz, A., 1977. Etude de Kérogènes par résonance paramagnétique électronique. In: *Advances in Organic Geochemistry 1975*. ENADIMSA, Madrid, pp. 753–779.
- Durand, B. (Ed.), 1980. *Kerogen, Insoluble Organic Matter from Sedimentary Rocks*. Éditions Technip, Paris, 519 pp.
- Egerton, R.F., 1989. *Electron Energy-Loss Spectroscopy in the Electron Microscope*. Plenum Press, New York.
- Faulon, J.L., Vandenbrouke, M., Drappier, J.M., Behar, F., Romero, M., 1989. 3D Chemical model for geological macromolecules. *Org. Geochem.* 16, 981–993.
- Garvie, L.A., Craven, A.J., Brydson, R., 1984. Use of electron-energy loss near-edge fine structure in the study of minerals. *Am. Mineralogist* 79, 411–425.
- Guignard, G., Thevenard, F., van Konijnenburg-van Cittert, J.H.A., 1998. Cuticle ultra structure of the cheirolepidiaceae conifer *Hirmeriella muensteri* (Schenk) Jung. *Rev. Palaeobot. Palynol.* 104 (2), 115–141.
- Harley, M.M., 1997. Ultra structure of pollen from some Eocene palm flowers (Messel, Germany). *Mededelingen Nederlands Instituut voor Toegepaste Geowetenschappen TNO* 58, 193–209.
- Hemsley, A.R., Glasspool, I.J., 1999. Megaspore ultra structure. In: Jones, T.P., Rowe, N.P. (Eds.), *Fossil Plants and Spores: Modern Techniques*. Geological Society of London, United Kingdom (GBR), London.
- House, C.H., Schopf, J.W., McKeegan, K.D., Coath, C.D., Harrison, T.M., Stetter, K.O., 2000. Carbon isotopic composition of individual Precambrian microfossils. *Geology* 28, 707–710.
- Jones, T.P., Rowe, N.P. (Eds.), 1999a. *Fossil Plants and Spores: Modern Techniques*. Geological Society of London, United Kingdom (GBR), London.
- Jones, T.P., Rowe, N.P., 1999b. Plant cell walls. In: Jones, T.P., Rowe, N.P. (Eds.), *Fossil Plants and Spores: Modern Techniques*. Geological Society of London, United Kingdom (GBR), London.
- Jones, T.P., Rowe, N.P., 1999c. Embedding techniques; adhesives and resins. In: Jones, T.P., Rowe, N.P. (Eds.), *Fossil Plants and Spores: Modern Techniques*. Geological Society of London, United Kingdom (GBR), London.
- Kazmierczak, J., Altermann, W., 2002. Neoproterozoic biomineralization by benthic coccoid cyanobacteria. *Science* 298, 2351.
- Kazmierczak, J., Kremer, B., 2002. Thermal alteration of the Earth's oldest fossils. *Nature* 420, 477–478.
- Kempe, A., 2003. *Nanostructures in Precambrian Fossils*. Geo-Bio-Nano, 1. Utz Verlag, Munich, Germany, 155 pp.
- Kempe, A., Schopf, J.W., Altermann, W., Kudryavtsev, A.B., Heckl, W.M., 2002. Atomic force microscopy of Precambrian microscopic fossils. *Proc. Natl. Acad. Sci. U.S.A.* 99 (14), 9117–9120.
- Kudryavtsev, A.B., Schopf, J.W., Agresti, D.G., Wdowiak, T.J., 2000. In situ laser-Raman imagery of Precambrian microscopic fossils. *Proc. Natl. Acad. Sci. U.S.A.* 98 (3), 823–826.
- Kwok, S., 2004. The synthesis of organic and inorganic compounds in evolved stars. *Nature* 430, 985–991.
- Loeblich Jr., A.R., 1970. Morphology, ultra structure and distribution of Paleozoic acritarchs. *Atti - Istituto Veneto di Scienze, Lettere ed Arti. Classe di Scienze Matematiche e Naturali* 70 (G), 705–788.
- Loeblich Jr., A.R., Drugg, W.S., 1968. New acritarchs from the Early Devonian (Late Gedinian) Haragan Formation of Oklahoma, USA. *Tulane Studies Geol.* 6 (4), 129–137.

- Loeblich Jr., A.R., Tappan, H., 1969. Acritarch excystment and surface ultra structure with descriptions of some Ordovician taxa. *Revista Espanola de Micropaleontologia* 1 (1), 45–57.
- Loeblich Jr., A.R., Tappan, H., 1971. New observations of the ultra structure of Asketopalla, an Ordovician acritarch. *J. Paleontol.* 45 (5), 899–901.
- Malis, T., Cheng, S.C., Egerton, R.F., 1988. EELS log-ratio technique for specimen thickness measurement in the TEM. *J. Electron Microsc. Technol.* 8, 193–200.
- Mapelli, C., Castiglioni, C., Meroni, E., Zerbi, G., 1999a. Graphite and graphitic compounds: vibrational spectra from oligomers to real materials. *J. Mol. Struct.* 480–481, 615–620.
- Mapelli, C., Castiglioni, C., Zerbi, G., Müllen, K., 1999b. Common force field for graphite and polycyclic aromatic hydrocarbons. *Phys. Rev. B* 60, 12710–12725.
- Moore, T.B., Schopf, J.W., 1992. Geographic and geologic data for PPRG rock samples. In: Schopf, J.W., Klein, C. (Eds.), *The Proterozoic Biosphere—A Multidisciplinary Study*. Cambridge University Press, Cambridge.
- Negri, F., Castiglioni, C., Tommasini, M., Zerbi, G., 2002. A computational study of the Raman spectra of large polycyclic aromatic hydrocarbons: toward molecularly defined subunits of graphite. *J. Phys. Chem. A* 106, 3306–3317.
- Oehler, D.Z., 1977. Pyrenoid-like structures in Late Precambrian algae from the Bitter Springs Formation. *J. Paleontol.* 51, 885–901.
- Osborn, J.M., Phipps, C.J., Taylor, T.N., Taylor, E.L., 2000. Structurally preserved sphenophytes from the Triassic of Antarctica; reproductive remains of *Spaciinodum*. *R. Palaeobot. Palynol.* 111 (3–4), 225–235.
- Rigolio, M., Castiglioni, C., Zerbi, G., Negri, F., 2001. Density functional theory prediction of the vibrational spectra of polycyclic aromatic hydrocarbons: effect of molecular symmetry and size on Raman intensities. *J. Mol. Struct.* 563–564, 79–87.
- Schopf, J.W., 1992a. Informal revised classification of proterozoic microfossils. In: Schopf, J.W., Klein, C. (Eds.), *The Proterozoic Biosphere—A Multidisciplinary Study*. Cambridge University Press, Cambridge, pp. 1119–1168.
- Schopf, J.W., 1992b. Proterozoic prokaryotes: affinities, geologic distribution, and evolutionary trends. In: Schopf, J.W., Klein, C. (Eds.), *The Proterozoic Biosphere—A Multidisciplinary Study*. Cambridge University Press, Cambridge, pp. 195–218.
- Schopf, J.W., 1993. Microfossils of the Early Archean Apex chert: new evidence for the antiquity of life. *Science* 260, 640–646.
- Schopf, J.W., 2004. Earth's earliest biosphere: status of the hunt. In: Eriksson, P.G., Altermann, W., Nelson, D.R., Mueller, W., Catuneanu, O. (Eds.), *The Precambrian Earth: Tempos and Events*. Developments in Precambrian Geology. Elsevier, pp. 516–539.
- Schopf, J.W., Czaja, A.D., Kudryavtsev, A.B., Agresti, D.G., Wdowiak, T.J., Kempe, A., Altermann, W., Heckl, W.M., 2002a. The oldest evidence of life, ISSOL meeting June 30–July 5, Oaxaca, Mexico.
- Schopf, J.W., Kudryavtsev, A.B., Agresti, D.G., Wdowiak, T.J., Czaja, A.D., 2002b. Laser-Raman imagery of Earth's earliest fossils. *Nature* 416 (7), 73–76.
- Schopf, J.W., Kudryavtsev, A.B., Agresti, D.G., Czaja, A.D., Wdowiak, T.J., 2005. Raman imagery: a new approach to assess the geochemical maturity and biogenicity of permineralized Precambrian fossils. *Astrobiology* 5, 333–371.
- Schopf, J.W., Oehler, D.Z., 1976. How old are the eukaryotes? *Science* 193, 47–49.
- Talyzina, N.M., 2000. Ultra structure and morphology of *Chuarina circularis* (Walcott, 1899) Vidal and Ford (1985) from the Neoproterozoic Visingso Group, Sweden. *Precambrian Res.* 102 (1/2), 123–134.
- Talyzina, N.M., Moczydlowska, M., 2000. Morphological and ultrastructural studies of some acritarchs from the Lower Cambrian Lukati Formation, Estonia. *R. Palaeobot. Palynol.* 112 (1–3), 1–21.
- Talyzina, N.M., Moldowan, J.M., Johannisson, A., Fago, F.J., 2000. Affinities of Early Cambrian acritarchs studied by using microscopy, fluorescence flow cytometry and biomarkers. *Rev. Palaeobot. Palynol.* 108 (1/2), 37–53.
- Taylor, T.N., 1999. The ultra structure of fossil cuticle. In: Jones, T.P., Rowe, N.P. (Eds.), *Fossil Plants and Spores: Modern Techniques*. Geological Society of London, United Kingdom (GBR), London.
- Vandebroucke, M., 2003. Kerogen: from types to models of chemical structure. *Oil & Gas Science and Technology - Rev. IFP* 58, 243–269.
- van Krevelen, D.W., 1993. *Coal: Typology–Chemistry–Physics–Constitution*, 3rd ed. Elsevier, Amsterdam, 979 pp.
- Wellman, C.H., Axe, L., 1999. In: Jones, T.P., Rowe, N.P. (Eds.), *Extracting plant mesofossils and megafossils by bulk acid maceration*. Geological Society of London, United Kingdom (GBR), Fossil plants and spores; modern techniques.
- Williamson, B.J., Jones, T.P., Berube, K.A., 1999. Calcareous algae; analytical techniques. In: Jones, T.P., Rowe, N.P. (Eds.), *Fossil Plants and Spores: Modern Techniques*. Geological Society of London, United Kingdom (GBR), London.
- Wirth, R., 2004. Focused Ion Beam (FIB): a novel technology for advanced application of micro- and nanoanalysis in geosciences and applied mineralogy. *Eur. J. Miner.* 16, 863–876.
- Yang, W., Zhang, H., Xu, F., 1998. A tentative study on the ultra structure of the Middle Permian acritarch *Michrhystridium* from western Yunnan, China. *Chin. Sci. Bull.* 43 (21), 1823–1826.